Int. J. Dynam. Control
DOI 10.1007/s40435-017-0344-4

Effect of the interaction between tool and workpiece modes on turning with round inserts

Firas A. Khasawneh[1] · **Andreas Otto**[2]

Received: 30 January 2017 / Revised: 29 May 2017 / Accepted: 13 June 2017

Abstract In this paper we investigate the effect of the tool-workpiece mode interaction on the stability of a flexible-tool, flexible-workpiece turning process. The workpiece dynamics are modeled by classical beam theory while for the tool we consider a description in terms of eigenmodes with an arbitrary orientation. The focus here is on elucidating the coupling effects due to the flexibility of both structures. Specifically, we show how the tool location along the workpiece and the dynamics of both the workpiece and the tool affect stability. Another contribution of this paper is the utilization of a novel analytical force model for cutting with round inserts. Using this force model, we further show that when round inserts are present, commonly used frequency domain methods can no longer be utilized to capture the system stability. Consequently, we use the spectral element approach, a highly-efficient time-domain approach, for studying the system stability.

Keywords Machining · Stability · Time-domain · Turning

1 Introduction

Regenerative chatter is one of the important challenges in metal removal processes [1]. Its detrimental effects on surface quality, tool wear, and machine/workpiece integrity has led to a large body of literature that aims to predict and avoid or quench its occurrence [2]. The majority of the work on chatter considers the case when the tool is flexible and the workpiece is rigid. On the other hand, the case of a rigid tool but flexible workpiece has received less attention which mostly focused on simulation and finite element modeling [3–6]. The case of machining a flexible workpiece is more challenging because the dynamic properties of the workpiece vary along the tool path. This is due to the change in the mass and stiffness of the workpiece and the influence of the location of the tool on the system dynamics. In addition, the deflections of the flexible workpiece are coupled to the cutting forces [7], and nonlinearities in stiffness and damping especially in milling have a strong influence on the dynamics of flexible thin-wall structures [8].

A force model based on the perfect plastic layer model for milling a flexible workpiece with a rigid tool was developed in [9]. This model was used to account for surface location errors due to static, chatter-free deflections. Some semi-analytical methods for the stability of flexible workpiece systems can be found in the literature. The majority of these studies use a frequency domain approach, usually the zero order approximation (ZOA) [10], to study the system stability. For example, a rough procedure for milling process planning of a flexible part was described in [11]. The non-uniform stiffness of the part at different locations of the workpiece was obtained using finite element approach while the stability calculations were obtained using ZOA. The surface location errors and milling stability of thin wall structures was studied in [12,13], respectively. The effect of the tool-to-workpiece offset in milling thin-wall structures was studied in [14] where discrepancies were reported between experimental data and the stability results from the ZOA. To capture the variation in the system dynamics of a flexible workpiece-rigid tool system, a third axis represent-

✉ Firas A. Khasawneh
khasawn3@msu.edu

Andreas Otto
otto.a@mail.de

[1] Department of Mechanical Engineering, Michigan State University, East Lansing, MI 48824, USA

[2] Institute for Physics, TU Chemnitz, 09107 Chemnitz, Germany

Published online: 29 June 2017

ing the location of the tool along the workpiece was added to the stability diagram in [15]. The stability analysis was performed using the ZOA and the workpiece was modeled as a single degree of freedom system. The authors asserted that their model was not suitable for machining flexible workpiece with a flexible tool.

The coupling effects in a flexible tool-flexible workpiece system were shown to be important in [12,16–19]. To account for the variation in the system dynamics in milling a flexible workpiece with a compliant tool, a third axis was added to the traditional stability lobes in [16]. The additional axis represented a different stage of milling corresponding to a different axial depth of cut. Only immersion angles of up to 90° were considered and the ZOA was used for stability analysis. The authors reported that simultaneously considering the stability of the tool and the workpiece is more accurate than superimposing the individual stability results for the tool and the workpiece. However, since the time domain information is lost in this approach, it is necessary to use an ad-hoc procedure to sift out the mode shapes that do not influence the cutting zone dynamics.

The frequency domain solution approach, e.g., via ZOA, is useful in many practical situations. However, a time domain approach is more accurate when the process is of highly intermittent nature [20–22]. Further, a time-domain approach is more advantageous when modeling complex cutter-part interactions or when the model includes time- or state- dependent delays [23]. Some of the time domain based methods for studying machining processes include semi-discretization [24,25], Chebyshev collocation [26–28], and finite element method [29–31]. The stability analysis of machining flexible structures was also studied using some of these methods.

For example, the stability of milling thin workpieces during finishing cuts with a rigid cutter was studied in [32] using the semi-discretization approach [33–35]. The authors used a finite element model to take into account the effect of material removal and the variation of the dynamic characteristics of the workpiece with the tool position. The variation of the geometry of the workpiece during cutting was ignored due to the small depth of finishing cuts. A model for milling thin-walled structures with long, compliant end mills was studied in [36]. The model took into account the flexibility of the workpiece but only along the axial depth of cut. The numerical stability analysis was performed using both ZOA and the semi-discretization approach. Semi-discretization was further used to simulate the model in time; however, the experimental validation was conducted assuming the workpiece was rigid and the tool was flexible.

Modeling of cutting processes of flexible structures thus remains a challenging problem. Further, models based on time-domain methods are few in comparison to the number of studies where the tool is assumed flexible whereas the workpiece is assumed rigid. This observation is true specifically for common machining processes such as milling and turning.

In this paper we investigate the effect of the tool-workpiece mode interaction on the stability of a turning operation where both the tool and the workpiece are flexible. It is assumed that workpiece dynamics can be modeled by Euler beam theory and tool dynamics can be described by modal parameters of the structure. We investigate the case of a round insert and utilize a novel analytical force model to capture its effect on the cutting process. We further show that when round inserts are present, the identification of the system stability with commonly used frequency domain methods is no longer applicable. Therefore, in this paper we use the spectral element approach to obtain the system stability [37]. We also show the equilibrium solution as a function of the tool location along the workpiece. The focus here is on elucidating the coupling effects due to the flexibility of both structures. Specifically, we show how the changing workpiece dynamics, due to a changing tool location, and the interaction between the workpiece and the tool dynamics affect stability.

We start by presenting the mechanical model in Sect. 2. The results of the stability analysis and the equilibrium solution calculation in terms of some of the important system parameters are introduced in Sect. 3, and the conclusions are included in Sect. 4.

2 Mechanical model

A turning process of a flexible-tool flexible-workpiece (FTFW) is shown in Fig. 1. The workpiece is assumed to be flexible in the x and y directions, while the tool is compliant in the x, y, and z directions. The structural dynamics for the tool and the workpiece are derived in Sects. 2.1 and 2.2, respectively. An analytical cutting force model for round inserts is introduced in Sect. 2.3, and the overall equation of motion is presented in Sect. 2.4.

2.1 Structural dynamics of the cutting tool

Let the 3×1 column vector $\mathbf{v}(t) = [v_x(t), v_y(t), v_z(t)]^T$ represent the tool tip position in the fixed Cartesian coordinate system shown in Fig. 1a. The tool tip position in Cartesian coordinates can be decomposed into modal displacements $\mathbf{q}_c(t)$ of the tool eigenmodes

$$\mathbf{v}(t) = \mathbf{V}_c\mathbf{q}_c(t), \tag{1}$$

where the columns of the $3 \times n_c$ matrix $\mathbf{V}_c$ contain the n_c structural mode shapes of the tool. The mode shapes of the tool are scaled in such a way that the modal masses are unity and the equation of motion for the tool dynamics can be written as

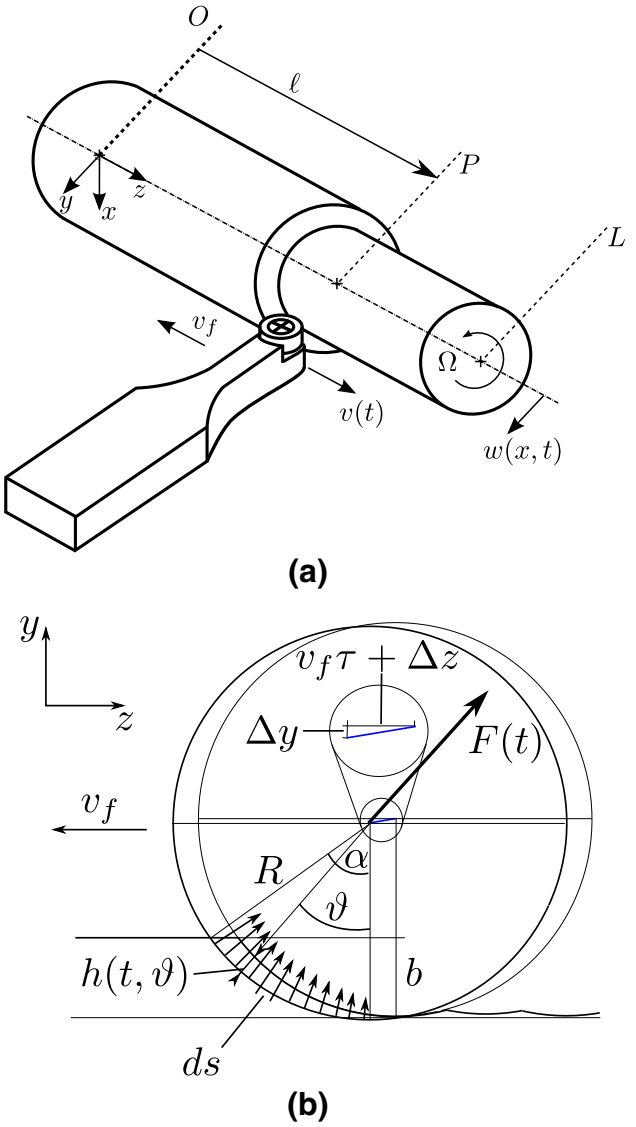

Fig. 1 **a** A schematic of the turning process of a flexible workpiece with a compliant tool. **b** The dynamic cutting force is assumed to be proportional to the *sickle-shaped* cross section of the chip created by a *vertical* and *horizontal* displacement Δy and $h_0 + \Delta z$ of the round *insert*

$$\ddot{\mathbf{q}}_c(t) + \mathbf{C}_c\dot{\mathbf{q}}_c(t) + \mathbf{K}_c\mathbf{q}_c(t) = \mathbf{V}_c^T\mathbf{F}(t), \tag{2}$$

where the $n_c \times n_c$ matrices

$$\mathbf{C}_c = \mathrm{diag}\big(\{2\zeta_i\omega_i\}_{i=1}^{n_c}\big), \quad \mathbf{K}_c = \mathrm{diag}\big(\{\omega_i^2\}_{i=1}^{n_c}\big), \tag{3}$$

are related to the damping and stiffness terms of the tool. The 3×1 column vector $\mathbf{F}(t)$ specifies the cutting force in Cartesian coordinates and the product $\mathbf{V}_c^T\mathbf{F}(t)$ represents the cutting force in modal coordinates. Note that the tool eigenmodes typically have arbitrary mode shapes in the xyz-space; therefore, depending on the mode shape, for example, forces in the x direction can cause vibrations in the z direction.

2.2 Structural dynamics of the workpiece

We assume that vibrations in the cutting force direction x do not affect the cutting force, i.e., they are only forced vibrations. Moreover, we assume that the workpiece is rigid in the axial direction z. Thus, we only consider the workpiece vibrations in y direction. Although the workpiece is a spinning rotor, other factors such as the gyroscopic effect are ignored since at the small velocities we are considering the gyroscopic effect is negligible for a cylindrical workpiece. Assuming that the workpiece is a long slender bar which can be modeled using the Euler–Bernoulli beam theory, the workpiece displacement $w(z,t)$ in the y direction, along the workpiece axis z, can be described according to

$$\rho A\frac{\partial^2 w(z,t)}{\partial t^2} + (EI)_y\frac{\partial^4 w(z,t)}{\partial z^4} = -F_y(z,t)\delta(z-\ell), \tag{4}$$

where ρ is the workpiece density, A is its cross sectional area, E is the modulus of elasticity, I is the cross-sectional area moment of inertia about an axis normal to x and y, δ is the Dirac delta function, and ℓ specifies the cutting location along the workpiece axis [38]. Other models can be used to characterize the dynamics of the workpiece such as the Timoshenko-Beam theory [39]. However, regardless of the used beam model, the subsequent analysis still holds.

Introducing a damping term to account for energy dissipation in the system, Eq. (4) can be written as

$$\begin{aligned}\rho A\frac{\partial^2 w}{\partial t^2}(z,t) + c_y\frac{\partial w}{\partial t}(z,t) + (EI)_y\frac{\partial^4 w}{\partial z^4}(z,t)\\ = -F_y(z,t)\delta(z-\ell).\end{aligned} \tag{5}$$

A modal expansion can be defined for w over the first n_w modes and it can be written according to

$$w(z,t) = \sum_{i=1}^{n_w}\psi_i(z)q_i(t) = \boldsymbol{\psi}(z)\mathbf{q}_w(t), \tag{6}$$

where $\boldsymbol{\psi}(z) = [\psi_1(z), \ldots, \psi_{n_w}(z)]$ are the modal vectors while $\mathbf{q}_w(t) = [q_1(t), \ldots, q_{n_w}(t)]^T$ are the generalized coordinates. Substituting the modal expansion Eq. (6) into Eq. (5) and integrating over the length L of the beam after pre-multiplying with $\boldsymbol{\psi}^T(z)$ gives

$$\ddot{\mathbf{q}}_w(t) + \mathbf{C}_w\dot{\mathbf{q}}_w(t) + \mathbf{K}_w\mathbf{q}_w(t) = \mathbf{V}_w^T(\ell)\mathbf{F}(t), \tag{7}$$

where the $3 \times n_w$ matrix $\mathbf{V}_w(\ell) = [\mathbf{0}; -\boldsymbol{\psi}(\ell); \mathbf{0}]$ contains the mode shapes of the workpiece at the cutting location ℓ. Note, that the mode shapes of the workpiece have no contributions in x- and z-direction since we neglect these displacement. In Eq. (7), without loss of generality, we have normalized the mode shapes such that

$$(\rho A)_y \int_0^L \boldsymbol{\psi}^T(z)\boldsymbol{\psi}(z)dz = \mathbf{I}_{n_w \times n_w}, \tag{8}$$

and the sampling property of the Dirac delta function was used,

$$\int_0^L \boldsymbol{\psi}^T(z)F_y(z,t)\delta(z-\ell)dz = \boldsymbol{\psi}^T(\ell)F_y(\ell,t) = \mathbf{V}_w^T(\ell)\mathbf{F}(t). \tag{9}$$

Due to the orthogonality of the workpiece eigenmodes, the $n_w \times n_w$ modal damping and modal stiffness matrices $\mathbf{C}_w$ and $\mathbf{K}_w$ are diagonal matrices given by

$$\mathbf{C}_w = \mathrm{diag}\left(\left\{2\zeta_{yi}\omega_{yi}\right\}_{i=1}^{n_w}\right), \quad \mathbf{K}_w = \mathrm{diag}\left(\left\{\omega_{yi}^2\right\}_{i=1}^{n_w}\right), \tag{10}$$

while the natural frequencies and the damping ratios for the ith mode can be given by

$$\omega_{yi}^2 = (EI)_y \int_0^L \psi_i^T(z)\psi_i''''(z)dz,$$
$$\zeta_{yi} = \frac{c_y}{2\omega_{yi}(\rho A)_y}. \tag{11}$$

In the next section we introduce a force model that will be used to define the right hand side of Eqs. (2) and (7).

2.3 Cutting force model for round inserts

The cutting force $\mathbf{F}(t)$ couples the motion of the tool and the workpiece and is assumed to be proportional to the instantaneous chip thickness h [40]. For round inserts the chip thickness varies along the cutting edge as can be seen in Fig. 1b. Thus, the macroscopic cutting force $\mathbf{F}(t)$ is composed of the infinitesimal local forces $d\mathbf{F}(t,\vartheta)$ along the engaged cutting edge

$$d\mathbf{F}(t,\vartheta) = K_t \begin{pmatrix} 1 \\ k_n\cos\vartheta \\ k_n\sin\vartheta \end{pmatrix} h(t,\vartheta)ds, \tag{12}$$

where K_t is the tangential cutting force coefficient, k_n is the ratio between the normal and the tangential cutting force, and ϑ specifies the angular position of the infinitesimal segment at the cutting edge (see Fig. 1b). It is assumed, that the direction of the local force $d\mathbf{F}(t,\vartheta)$ is parallel to the radial direction of the insert. The chip thickness $h(t,\vartheta)$ is measured in the same direction and is given by

$$h(t,\vartheta) = \Delta y(t)\cos\vartheta + \Delta z(t)\sin\vartheta = [0\cos\vartheta\ \sin\vartheta]\Delta\mathbf{r}(t). \tag{13}$$

In Eq. (13), the vector $\Delta\mathbf{r}(t) = [\Delta x(t), \Delta y(t), \Delta z(t)]^T$ represents the relative displacements between the tool and the workpiece. Only the relative displacements in the y and the z direction between two subsequent cuts affect the chip thickness. The relative displacements in Eq. (13) are given by

$$\Delta x(t) = v_x(t-\tau) - v_x(t), \tag{14}$$
$$\Delta y(t) = v_y(t-\tau) - v_y(t) + w(\ell, t-\tau) - w(\ell,t), \tag{15}$$
$$\Delta z(t) = v_z(t-\tau) - v_z(t) + v_f\tau, \tag{16}$$

where τ is the period for one spindle revolution and v_f is the feed velocity. In Eq. (14) the term $v_f\tau$ specifies the static part of the displacement, i.e. the feed per one spindle revolution. Substituting Eq. (13) into Eq. (12) and using $ds = Rd\vartheta$, where R is the tool radius, leads to the matrix vector form for the local cutting force

$$d\mathbf{F}(t,\vartheta) = K_t R \begin{bmatrix} 0 & \cos\vartheta & \sin\vartheta \\ 0 & k_n\cos^2\vartheta & k_n\sin\vartheta\cos\vartheta \\ 0 & k_n\sin\vartheta\cos\vartheta & k_n\sin^2\vartheta \end{bmatrix} \Delta\mathbf{r}(t)d\vartheta. \tag{17}$$

The cutting force coefficient K_t and the ratio k_n are usually determined experimentally. The macroscopic cutting force $\mathbf{F}(t)$ is the integral of the local forces $d\mathbf{F}(t,\vartheta)$ along the cutting edge from $\vartheta = 0$ up to the engagement angle $\vartheta = \alpha$

$$\mathbf{F}(t) = \int_0^\alpha d\mathbf{F}(t,\vartheta) = K_t b\boldsymbol{\Xi}(\alpha)\Delta\boldsymbol{r}(t), \tag{18}$$

where in Eq. (18) we have used the condition

$$\cos\alpha = 1 - \frac{b}{R} \tag{19}$$

which relates the engagement angle α to the depth of cut b. The first column of the matrix $\boldsymbol{\Xi}(\alpha)$ is zero because displacements in x-direction do not affect the cutting force

$$\boldsymbol{\Xi}(\alpha) = \begin{bmatrix} 0 & a_{xy} & a_{xz} \\ 0 & a_{yy} & a_{yz} \\ 0 & a_{zy} & a_{zz} \end{bmatrix}, \tag{20}$$

while the remaining entries, i.e. the remaining directional factors a_{ij}, are given by

$$a_{xy} = \frac{\sin\alpha}{(1-\cos\alpha)}, \ a_{xz} = 1, \ a_{yy} = k_n\frac{2\alpha+\sin 2\alpha}{4(1-\cos\alpha)},$$
$$a_{yz} = a_{zy} = k_n\frac{1-\cos 2\alpha}{4(1-\cos\alpha)}, \ a_{zz} = k_n\frac{2\alpha-\sin 2\alpha}{4(1-\cos\alpha)}. \tag{21}$$

Note that the directional factors depend nonlinearly on the depth of cut b because, according to Eq. (19), the engagement angle α changes nonlinearly with the depth of cut b.

2.4 Equation of motion

The dynamics of the machining system shown in Fig. 1 can be described by the modal displacements $\mathbf{q}$ and mode shapes $\mathbf{V}$ as

$$\mathbf{q}(t) = \begin{bmatrix} \mathbf{q}_c(t) \\ \mathbf{q}_w(t) \end{bmatrix}, \quad \mathbf{V}(\ell) = \left[\mathbf{V}_c, \mathbf{V}_w(\ell)\right]. \tag{22}$$

Thus, we can write for the relative displacements between the tool and the workpiece

$$\Delta\mathbf{r}(t) = \mathbf{V}(\ell)\Delta\mathbf{q}(t) + \begin{bmatrix} 0 \\ 0 \\ v_f\tau \end{bmatrix}, \tag{23}$$

where $\Delta\mathbf{q} = \mathbf{q}(t-\tau) - \mathbf{q}(t)$. Consequently, substituting the force model (18) into Eqs. (2) and (7) for the tool and the workpiece dynamics, and assuming that the tool does not lose contact with the workpiece, gives

$$\ddot{\mathbf{q}}(t) + \mathbf{C}\dot{\mathbf{q}}(t) + \mathbf{K}\mathbf{q}(t) = \mathbf{q}_0(\ell,\alpha) + \mathbf{D}(\ell,\alpha)\Delta\mathbf{q}(t), \tag{24}$$

where the coefficient matrices read

$$\mathbf{C} = \begin{bmatrix} \mathbf{C}_c & \mathbf{0}_{n_c\times n_w} \\ \mathbf{0}_{n_w\times n_c} & \mathbf{C}_w \end{bmatrix}, \quad \mathbf{K} = \begin{bmatrix} \mathbf{K}_c & \mathbf{0}_{n_c\times n_w} \\ \mathbf{0}_{n_w\times n_c} & \mathbf{K}_w \end{bmatrix},$$
$$\mathbf{D}(\ell,\alpha) = K_t b \mathbf{V}^T(\ell)\boldsymbol{\Xi}(\alpha)\mathbf{V}(\ell), \tag{25}$$

and the static cutting force in modal coordinates can be described by

$$\mathbf{q}_0(\ell,\alpha) = K_t b \mathbf{V}^T(\ell)\boldsymbol{\Xi}(\alpha)\begin{bmatrix} 0 \\ 0 \\ v_f\tau \end{bmatrix}. \tag{26}$$

Defining the $2(n_w + n_c)$ vector $\mathbf{s} = [\mathbf{q}; \dot{\mathbf{q}}]$, Eq. (24) can be written according to

$$\dot{\mathbf{s}}(t) = \mathbf{A}\mathbf{s}(t) + \mathbf{B}\mathbf{s}(t-\tau) + \mathbf{s}_0, \tag{27}$$

where

$$\mathbf{A} = \begin{bmatrix} \mathbf{0}_{(n_w+n_c)} & \mathbf{I}_{(n_w+n_c)} \\ -\mathbf{K}-\mathbf{D} & -\mathbf{C} \end{bmatrix}, \mathbf{B} = \begin{bmatrix} \mathbf{0}_{(n_w+n_c)} & \mathbf{0}_{(n_w+n_c)} \\ \mathbf{D} & \mathbf{0}_{(n_w+n_c)} \end{bmatrix},$$
$$\mathbf{s}_0 = \begin{bmatrix} \mathbf{0}_{(n_w+n_c)} \\ \mathbf{q_0} \end{bmatrix}. \tag{28}$$

The size of square matrices $\mathbf{A}$ and $\mathbf{B}$ is $2(n_w + n_c)$ while the size of the column vector $\mathbf{s}_0$ is $2(n_w+n_c)$; therefore, it can be seen that the size of the state matrices becomes large as the number of tool modes and/or workpiece modes is increased.

For the specific form of the cutting force in Eq. (20), we notice that the dynamics in the x-direction only represent forced vibrations and they do not have an effect on the cutting force. Therefore, we can neglect the vibrations along x in the stability analysis. Note that these vibrations cannot be ignored in the following cases:

1. The entries in the first column in the matrix of the directional factors Eq. (20) are non-zero, i.e. x-vibrations affect the cutting force.
2. The cutting force is velocity dependent ($\dot{x}$ affects the cutting force).

Since the cross frequency response functions (FRFs) of the workpiece dynamics are zero, i.e. the displacements in the y-direction only depend on the excitation in the same direction, only the excitation in the y-direction is considered for the workpiece dynamics [see the definition of the matrix $\mathbf{V}_w(\ell)$ in Sect. 2.2]. In contrast, on the machine-tool side, the cross FRFs are not zero. For example, an excitation in the x-direction can lead to a response not only in the x-direction but also in the y-direction. Therefore, the tool excitation in the three Cartesian coordinates must be taken into account and a 3-dimensional model must be used to characterize the tool response.

3 Results and discussion

The stability of Eq. (27) is studied using the spectral element approach [37] for two different sets of parameters in Sects. 3.1 and 3.2. The results of Sect. 3.1 highlight the interaction between the modes of the tool and the workpiece for a theoretical model, while Sect. 3.2 investigates the stability of a model with more realistic parameters. Section 3.3 comments on the limitations that the force model introduces into some frequency domain methods for the stability analysis.

Since the term $\mathbf{s}_0$ does not affect the stability of the system, we will drop it from the stability analysis of Eq. (27). More precisely, the vector $\mathbf{s}_0$ in Eq. (27) contains the static component of the cutting force that is responsible for the static deflection of the tool as well as the surface location error between the commanded position and the actual position of the tool relative to the workpiece during a stable cut. The static deflection between the tool and the workpiece $\mathbf{s}_{\text{eq}}$ is calculated in Sect. 3.2 for the model with realistic parameters. Specifically, the static deflection corresponds to $\dot{\mathbf{s}}_{\text{eq}} = 0$ and $\mathbf{s}_{\text{eq}}(t) = \mathbf{s}_{\text{eq}}(t-\tau)$. Making this substitution in Eq. (27) gives

$$\mathbf{s}_{\text{eq}}(\ell,\alpha) = -(\mathbf{A}+\mathbf{B})^{-1}\mathbf{s}_0(\ell,\alpha). \tag{29}$$

Table 1 The parameters used in the turning model

Process parameters	$K_t = 1000 \times 10^6 \text{N/m}^2$	$k_n = 0.3$	$v_f \tau = 0.12$ mm
Workpiece parameters	$\rho = 2700$ kg/m^3	$\zeta_y = 0.03$, $\omega_y = 792$ Hz	L=0.25 m, D=0.07 m
Boundary conditions	fixed-free		
Cutting tool parameters			
$\zeta = 0.03$	$\omega = \omega_r \times \omega_y$ Hz	$\omega_r \in \{0.5, 0.7, 0.9, 1.1, 1.3, 1.5\}$	$R = 8$ mm
$\mathbf{V} = \begin{bmatrix} \frac{3}{\sqrt{10}} \\ 0 \\ \frac{1}{\sqrt{10}} \end{bmatrix}$	$K_r = 10 \times 10^6$ N/m	$M_r = K_r/\omega^2$	

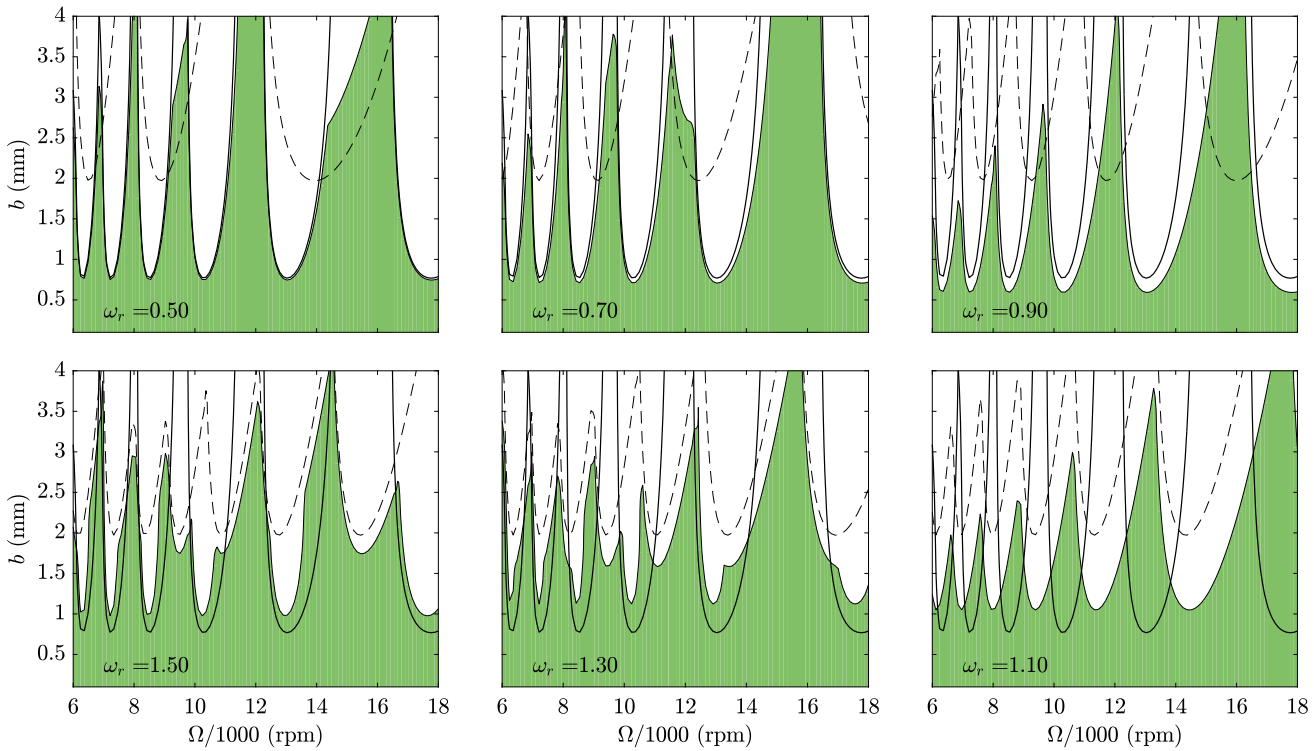

Fig. 2 Stability lobe diagrams for parameters from Table 1 with $\ell = L$ and variable values of the ratio $\omega_r = \omega/\omega_y$ between tool and workpiece eigenfrequency. The *shaded area* shows the stability region for the FTFW system. The superimposed *solid black* and *dashed line* show the isolated workpiece stability and the isolated tool stability, respectively. The figure shows that, in general, in the FTFW system due to the mode interaction the mode with the lower eigenfrequency is stabilized by the mode with the higher eigenfrequency

The corresponding equilibrium solution in Cartesian coordinates is a 3×1 column vector $\mathbf{r}_{\text{eq}}$ obtained according to

$$\mathbf{r}_{\text{eq}}(\ell, \alpha) = \left[\mathbf{V}(l), \mathbf{0}_{3\times(n_w+n_c)}\right] \mathbf{s}_{\text{eq}}(\ell, \alpha), \tag{30}$$

which specifies the static deflection between the tool and the workpiece for cutting at location ℓ with engagement angle α.

3.1 Effect of mode interaction on stability

We investigate the effect of the tool-workpiece mode interaction by first studying a theoretical model with one dominant workpiece eigenmode and one dominant eigenmode of the tool with the parameters shown in Table 1. The eigenfrequency ω_y of the workpiece mode is fixed and determined from the workpiece parameters. In contrast, the eigenfrequency of the tool ω is varied, where ω_r specifies the ratio of the tool and the workpiece eigenfrequency. Figure 2 shows the resulting stability diagrams for the FTFW system (shaded) when cutting at the free end of the workpiece $\ell = L$ for different frequency ratios ω_r. For illustrating the effect of the mode interaction, the figure also shows the stability boundaries associated with cutting using a rigid tool but flexible workpiece (solid line) which we will refer to as the isolated workpiece stability, and flexible tool but rigid workpiece (dashed line) which we will refer to as the iso-

lated tool stability. The isolated workpiece stability (solid line) remains constant because the parameters of the workpiece dynamics do not change in Fig. 2. In contrast, the width and the horizontal position of the isolated tool stability lobes change with varying ω_r but the lowest stability limit remains constant because the stiffness and the damping of the tool eigenmode is constant in Fig. 2.

In particular, for $\omega_r < 1$, i.e. the eigenfrequency of the tool is smaller than the eigenfrequency of the workpiece, the tool dynamics is stabilized significantly, whereas the workpiece dynamics is destabilized slightly. This can be seen by comparing the stability lobes of the FTFW system (shaded) with the isolated tool (dashed lobes) and the isolated workpiece stability (solid lobes). The effect becomes larger for $\omega_r \to 1$. For $\omega_r = 0.90$ no stability lobes corresponding to an unstable tool eigenmode can be found. In contrast, for $\omega_r > 1$ the tool eigenmode is destabilized, whereas the workpiece eigenmode is stabilized. Again, the effect is larger the closer the frequency ratio ω_r approaches one. For $\omega_r = 1.10$ the stability lobes from the flexible workpiece completely vanish. The mode interaction can be explained by considering the frequency domain approach for the system with two dominant eigenmodes. It is known that for turning the negative real part of the oriented transfer function specifies the limiting depth of cut [41,42]. For the example in this section the oriented transfer function of the FTFW system is simply a superposition of the FRFs of the isolated tool and the isolated workpiece mode. Since the real part of the FRFs of a single mode is positive for frequencies smaller than its eigenfrequency, in the superposed oriented transfer function for turning the eigenmodes with a smaller eigenfrequency are stabilized by the positive real part from eigenmodes with larger eigenfrequenies. However, if the mode with lower eigenfrequency is stabilized, this means that the mode with the higher eigenfrequency gets destabilized because at that chatter frequency both real parts are negative. In fact, this can be seen in Fig. 2, where the mode with the lower eigenfrequency is stabilized by the mode with the larger eigenfrequency. Due to the shape of the real part of a single mode FRFs the effect of the mode interaction is larger if the eigenfrequencies are closer to each other. In general. the results show that the stability of the FTFW system cannot be correctly captured by a simple superposition of the isolated tool and workpiece modes' stability, which is in agreement with the results shown in [16,41].

Whereas the above-mentioned example describes the general mode interaction in turning, in FTFW systems the interaction with the workpiece eigenmode depends on the cutting location ℓ. Figure 3 shows the stability diagrams for the FTFW system using two values of ω_r and three cutting locations along the axial direction of the workpiece denoted by ℓ. Again, the dashed curve in Fig. 3 shows the isolated tool stability. For $\ell = 0.25L$, the cutting location is very close to the chuck and the stability lobes of the FTFW system coincide with the isolated tool stability. This means that the flexibility of the workpiece does not change the stability. For $\ell = 0.75L$ no instability due to the workpiece flexibility exists, but the interaction between the dominant tool and the dominant workpiece modes can be seen in the location of the stability lobes of the tool for the FTFW system in comparison to the isolated tool stability. Again, the tool eigenmode is stabilized (destabilized) for $\omega_r = 0.6 < 1$ ($\omega_r = 1.4 > 1$). For $\ell = L$ the stabilizing and destabilizing effect due to the flexible workpiece is much larger. However, in this case the unstable workpiece vibrations lead to the emergence of additional lobes in the stability diagram.

3.2 Realistic model—stability and static deflection

In Fig. 4 the stability lobes for a more realistic example where the workpiece is fixed at one end and free at the other are presented. The workpiece parameters for the realistic example in this section are similar to the parameters used in Sect. 3.1 except for the inclusion of the workpiece's second bending mode in the analysis. The approach we describe here is capable of incorporating a high number of eigenmodes in the analysis. Nevertheless, our results show that the influence of the second bending mode on the stability lobes is negligible; therefore, we only include the first two workpiece eigenmodes in the analysis. The cutting location is specified by $\ell = L$ corresponding to the free end of the workpiece, and three dominant eigenmodes for the tool dynamics are taken into account. The parameters used in the analysis are given in Table 2.

Consistent with the results on the mode interaction in Sect. 3.1, instabilities corresponding to eigenmodes with lower eigenfrequencies are stabilized by eigenmodes with higher eigenfrequencies. In particular, the largest stabilization can be seen between 6000 and 7000 rpm, where the stability limit of the FTFW system is much higher than the broad lobe from the isolated tool stability. In general, a broader stability lobe corresponds to an eigenmode with a lower eigenfrequency. This means, that the isolated tool lobe between 6000 and 7000 rpm corresponds to the low frequency tool eigenmodes, and therefore, is significantly stabilized by the bending modes of the workpiece. The remaining stability lobes of the isolated tool stability correspond to the 1200 Hz mode. This high-frequency tool mode is slightly destabilized by the workpiece dynamics because its eigenfrequency is higher than the eigenfrequency of the dominant bending mode of the workpiece. On the other hand, the stability lobes associated with the dominant bending mode of the workpiece is stabilized by the 1200 Hz mode of the tool.

By examining the equilibrium solution in Eq. (29), it can be seen that the static displacements depend linearly on the

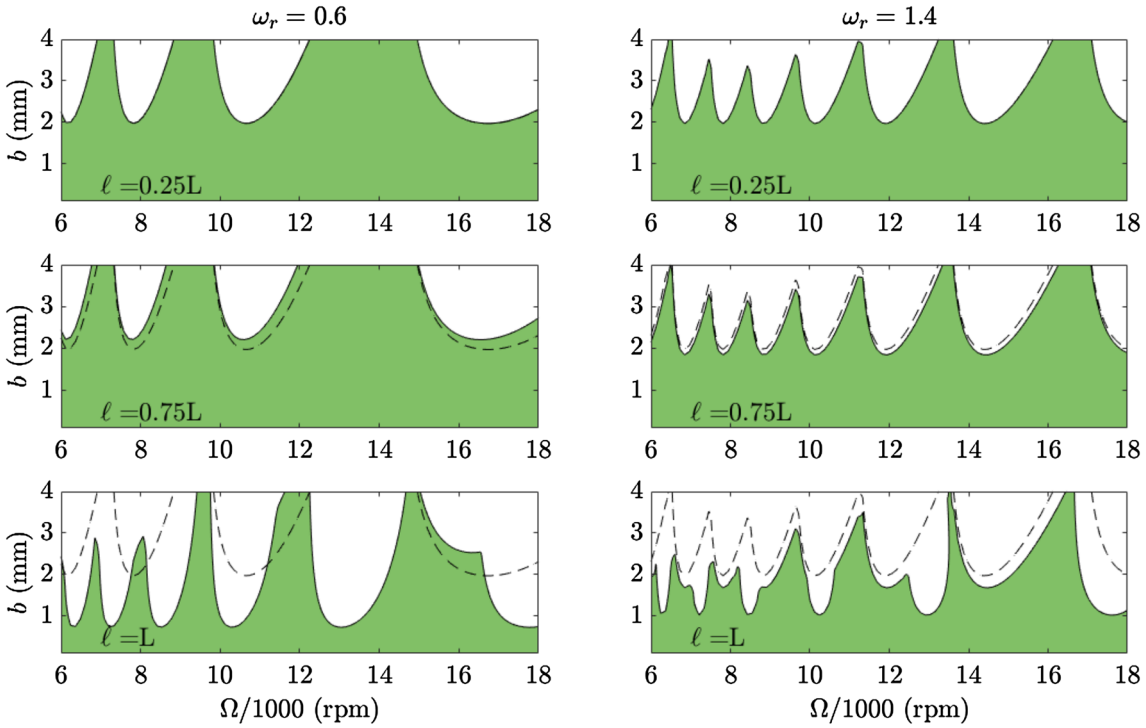

Fig. 3 Stability lobe diagrams for parameters from Table 1 with $\omega_r = 0.6$ (*left column*) and $\omega_r = 1.4$ (*right column*), and varying values of the cutting location ℓ. The *shaded region* shows the chatter-free area of the FTFW system while the *dashed black line* corresponds to the isolated tool stability. Whereas for the cutting location close to the chuck at $\ell = 0.25L$ the effect of the workpiece flexibility on the stability is negligible, the effect of the mode interaction increases for increasing values of ℓ, i.e., as the cutting location gets closer to the free end of the workpiece

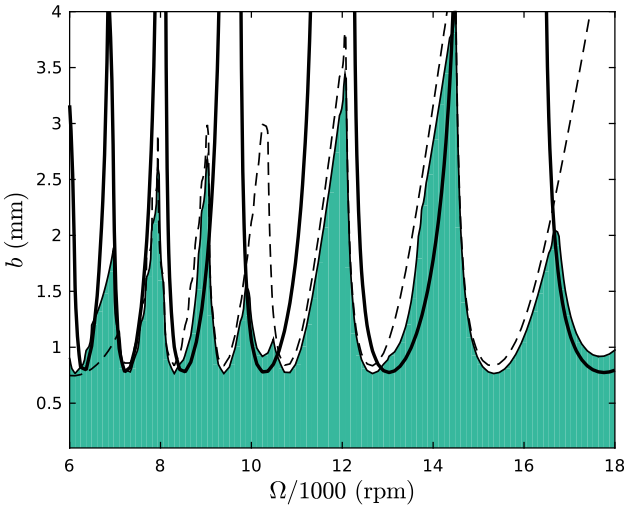

Fig. 4 Stability lobe diagrams for the realistic turning process where the parameters in Table 2 are used. The *shaded area* shows the stability region for the FTFW system. The superimposed *solid* and *dashed black line* show the stability of the isolated workpiece and isolated tool stability, respectively. It can be seen that broader lobes associated to modes with a lower eigenfrequency are stabilized by modes with higher eigenfrequencies

feed rate $v_f\tau$. It can also be seen that if the feed rate is constant, the static displacement does not depend on the spindle speed. The equilibrium solution y_{eq} for the FTFW system described by Eq. (30) and Table 2, which is relevant to the surface location error on the workpiece, is shown in Fig. 5. Specifically, Fig. 5a shows the equilibrium solution for the workpiece in the y-direction as a function of the cutting location ℓ for two values of the depth of cut b. For comparison, the scaled mode shapes are superimposed on the same plot in black dashed lines. It can be seen that the workpiece's static displacement in the y-direction increases with increasing the distance of the tool location from the chuck—similar to the behavior of the mode shape. Figure 5b shows a plot of y_{eq} for two constant cutting locations as a function of the depth of cut b, which clearly shows a nonlinear dependence of the equilibrium solution y_{eq} on the depth cut b. This is due to the fact that for round inserts the static cutting force increase nonlinearly with the depth of cut because of the nonlinear behavior of the directional factors described by Eqs. (19) and (21).

Table 2 The parameters used in the realistic turning example 1

Workpiece parameters	$\rho = 2700$ kg/m^3	$\zeta_y = (0.03, 0.0334)$ $\boldsymbol{\omega}_y = \text{diag}(792, 4964)$ Hz	L = 0.25 m, D = 0.07 m
Boundary conditions	fixed-free		
Cutting tool parameters			
$\boldsymbol{\zeta} = \text{diag}(0.03, 0.025, 0.01)$	$\omega = \text{diag}(75, 200, 1200)$ Hz	$R = 8$ mm	
$\mathbf{V} = \begin{bmatrix} \frac{2}{14} & 0 & \frac{1}{\sqrt{2}} \\ \frac{3}{14} & \frac{1}{\sqrt{2}} & 0 \\ \frac{1}{14} & \frac{1}{\sqrt{2}} & \frac{1}{\sqrt{2}} \end{bmatrix}$	$\mathbf{K}_r = \text{diag}(3.5, 10, 2.25) \times 10^7$ N/m	$\mathbf{M}_r = \mathbf{K}/\boldsymbol{\omega}$	

The process parameters that were used are identical to the ones shown in table

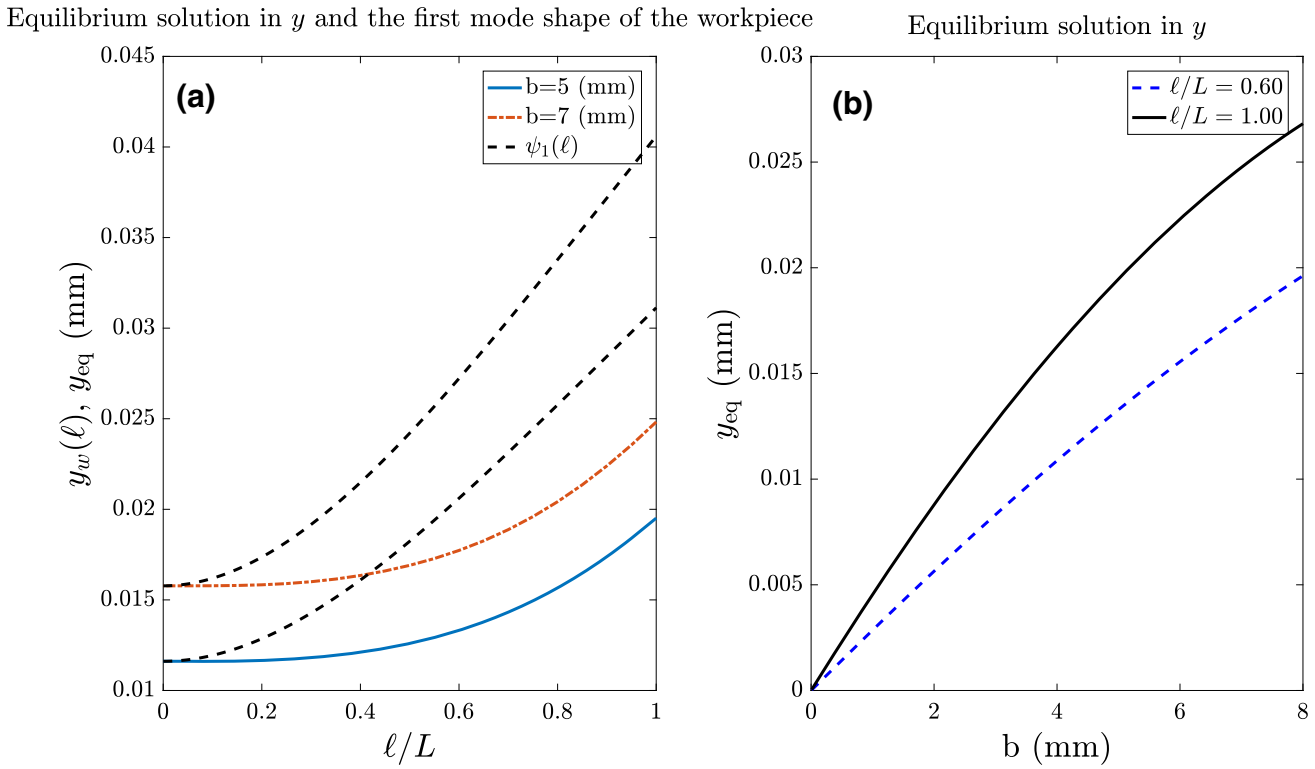

Fig. 5 The equilibrium solution y_{eq} calculated using Eq. (30) and the parameters in Table 2. **a** Shows the equilibrium solution as a function of the normalized cutting location ℓ/L for two values of b. The *dashed lines* superimpose the scaled and shifted dominant mode shape of the workpiece $\psi_1(\ell)$. In order to compare the mode shapes with the corresponding equilibrium solutions, the mode shapes were scaled first such that their maximum value is equal to the maximum value of the corresponding equilibrium solution. The mode shapes were then shifted vertically so that their start point coincides with that of the equilibrium solution. **b** Shows the equilibrium solution as a function of the depth of cut b for two values of ℓ/L

3.3 Round insert force model and frequency domain methods

The stability analysis results in this study were obtained using the spectral element method (SEA), a time domain approach. Interestingly, the same stability analysis cannot be performed using Tlusty's law, a frequency domain approach [42]. Tlusty's law and many other frequency domain approaches use the shortcut that the cutting force direction does not change for increasing depth of cut and the modulus of the cutting force is proportional to the depth of cut b. This is no longer true for the new force model for round inserts due to the nonlinear dependence of the directional factors in the cutting force term on the cutting depth, see Eqs. (19)–(21). In this case, similar to the SEA approach, it is necessary to determine the process stability for each pair of values of spindle speed and depth of cut separately.

4 Conclusions

This paper investigates the coupling effects between the tool and the workpiece in turning with a round insert when both the tool and the workpiece are flexible. Our results confirm that the stability of the FTFW system cannot be ascertained by superimposing the individual stability of the tool and that of the workpiece. To elaborate, the stability results in Figs. 2 and 4 show that, in general, the mode with the lower eigenfrequency is stabilized by the mode with the higher eigenfrequency. Specifically, when the eigenfrequency of the tool is smaller than that of the workpiece, the tool dynamics is stabilized significantly, whereas the workpiece dynamics is destabilized slightly. In contrast, when the eigenfrequency of the tool is larger than that of the workpiece, the tool eigenmode is destabilized, whereas the workpiece eigenmode is stabilized. In both cases, the corresponding effect becomes larger as the ratio ω_r of the eigenfrequency of the tool to that of the workpiece approaches one.

The specific contribution of the workpiece mode is dependent on the tool location during the cut. Specifically, Fig. 3 shows that as the tool gets farther from the fixed end of the workpiece, the interaction between the modes of the tool and the workpiece becomes stronger as evidenced by the stabilization (for $\omega_r < 1$) and the destabilization (for $\omega_r > 1$) of the isolated tool stability.

An investigation of the equilibrium solution y_{eq} in Fig. 5a shows that, similar to the workpiece eigenmode, the workpiece's static displacement increases with increasing values of ℓ. Further, Fig. 5 shows that the equilibrium solution varies nonlinearly with the depth of cut b. This nonlinear behavior is due to the nonlinearity in b in the expressions of the directional factors in Eq. (21).

Both the stability results and the equilibrium solution for the FTFW system were obtained using the spectral element approach—a time domain approach. The use of a time domain approach in this case was necessitated by the utilization of the force model for round inserts introduced in Sect. 2.3. This force model introduces a nonlinear dependence of the directional factors in the cutting force term on the cutting depth b. Consequently, this precludes using frequency domain methods which utilize the shortcut that the cutting force direction does not change for increasing depth of cut and the modulus of the cutting force is proportional to the depth of cut b.

In practice, not only the dynamics of the workpiece but also the tool dynamics (eigenmodes of the tool) vary with the cutting location. However in turning of flexible workpieces we assume that the variation of the workpiece dynamics is much larger than the variation of the tool eigenmodes. Hence, we consider invariant eigenmodes of the tool, which can be determined at an intermediate position of the tool path. For a more accurate analysis a position-dependent dynamic model of the machine tool can be found in [43,44].

Finally, for aggressive cutting, note that the removed material can affect the dynamic behavior of the workpiece. This means that the cutting process is stable for some tool locations and unstable for other tool locations. This effect was not considered in this manuscript, however, this is a topic that the authors plan to pursue in future work.

References

1. Tobias SA, Fishwick W (1958) Theory of regenerative machine tool chatter. Engineering 205:199–203
2. Quintana G, Ciurana J (2011) Chatter in machining processes: a review. Int J Mach Tools Manuf 51(5):363–376. doi:10.1016/j.ijmachtools.2011.01.001
3. Arnaud L, Gonzalo O, Seguy S, Jauregi H, Peigne G (2011) Simulation of low rigidity part machining applied to thin-walled structures. Int J Adv Manuf Technol 54(5–8):479–488. doi:10.1007/s00170-010-2976-9
4. Gang L (2009) Study on deformation of titanium thin-walled part in milling process. J Mater Proc Technol 209(6):2788–2793
5. Mehdi K, Rigal J, Play D (2002) Dynamic behavior of a thin-walled cylindrical workpiece during the turning process, part 1: cutting process simulation. J Manuf Sci Eng 124(3):562–568. doi:10.1115/1.1431260
6. Yu SD, Shah V (2009) Theoretical and experimental studies of chatter in turning for uniform and stepped workpieces. J Vib Acoust 130(6):061,005
7. Sutherland JW, DeVor RE (1986) An improved method for cutting force and surface error prediction in flexible end milling systems. J Manuf Sci Eng 108(4):269–279. doi:10.1115/1.3187077
8. Davies M, Balachandran B (2000) Impact dynamics in milling of thin-walled structures. Nonlinear Dyn 22(4):375–392. doi:10.1023/A:1008364405411
9. Ratchev S, Liu S, Huang W, Becker A (2004) A flexible force model for end milling of low-rigidity parts. J Mater Process Technol 153:134–138. doi:10.1016/j.jmatprotec.2004.04.300
10. Altintaş Y, Budak E (1995) Analytical prediction of stability lobes in milling. CIRP Ann 44(1):357–362
11. Lan JVL, Marty A, Debongnie JF (2007) Providing stability maps for milling operations. Int J Mach Tools Manuf 47(9):1493–1496
12. Budak E (2006) Analytical models for high performance milling. Part i: cutting forces, structural deformations and tolerance integrity. Int J Mach Tools Manuf 46(12–13):1478–1488. doi:10.1016/j.ijmachtools.2005.09.009
13. Tongyue W, Ning H, Liang L (2010) Stability of milling of thin-walled workpiece. In: 2010 international conference on mechanic automation and control engineering (MACE), pp 3408–3411. doi:10.1109/MACE.2010.5536868
14. Wanner B, Eynian M, Beno T, Pejryd L (2012) Process stability strategies in milling of thin-walled inconel 718. In: AIP conference proceedings, vol 1431, no 1, pp 465–472. doi:10.1063/1.4707597
15. Thevenot V, Arnaud L, Dessein G, Cazenave-Larroche G (2006) Influence of material removal on the dynamic behavior of thin-walled structures in peripheral milling. Mach Sci Technol 10(3):275–287
16. Bravo U, Altuzarra O, de Lacalle LL, Sanchez J, Campa F (2005) Stability limits of milling considering the flexibility of the workpiece and the machine. Int J Mach Tools Manuf 45(15):1669–1680
17. Chen C, Tsao Y (2006) A stability analysis of turning a tailstock supported flexible work-piece. Int J Mach Tools Manuf 46(1):18–25. doi:10.1016/j.ijmachtools.2005.04.002

18. Chen CK, Tsao YM (2006) A stability analysis of regenerative chatter in turning process without using tailstock. Int J Adv Manuf Technol 29(7–8):648–654
19. Vela-Martinez L, Jauregui-Correa J, Rubio-Cerda E, Herrera-Ruiz G, Lozano-Guzmï£.n A (2008) Analysis of compliance between the cutting tool and the workpiece on the stability of a turning process. Int J Mach Tools Manuf 48(9):1054–1062 Cited By (since 1996)19
20. Khasawneh FA, Bobrenkov OA, Mann BP, Butcher EA (2012) Investigation of period-doubling islands in milling with simultaneously engaged helical flutes. J Vib Acoust 134(2):021,008. doi:10.1115/1.4005022
21. Patel BR, Mann BP, Young KA (2008) Uncharted islands of chatter instability in milling. Int J Mach Tools Manuf 48:124–134
22. Szalai R, Stépán G (2006) Lobes and lenses in the stability chart of interrupted turning. J Comput Nonlinear Dyn 1:205–211
23. Altintas Y, Stepan G, Merdol D, Dombovari Z (2008) Chatter stability of milling in frequency and discrete time domain. CIRP J Manuf Sci Technol 1(1):35–44. doi:10.1016/j.cirpj.2008.06.003
24. Insperger T, Barton DA, Stepan G (2008) Criticality of hopf bifurcation in state-dependent delay model of turning processes. Int J Nonlinear Mech 43(2):140–149. doi:10.1016/j.ijnonlinmec.2007.11.002
25. Insperger T, Stepan G (2004) Stability analysis of turning with periodic spindle speed modulation via semidiscretization. J Vib Control 12:1835–1855. doi:10.1177/1077546304044891
26. Bobrenkov O, Khasawneh F, Butcher E, Mann B (2010) Analysis of milling dynamics for simultaneously engaged cutting teeth. J Sound Vib 329(5):585–606. doi:10.1016/j.jsv.2009.09.032
27. Butcher E, Bobrenkov O, Bueler E, Nindujarla P (2009) Analysis of milling stability by the Chebyshev collocation method: algorithm and optimal stable immersion levels. J Comput Nonlinear Dyn 4(3):031,003
28. Totis G, Albertelli P, Sortino M, Monno M (2014) Efficient evaluation of process stability in milling with spindle speed variation by using the Chebyshev collocation method. J Sound Vib 333(3):646–668. doi:10.1016/j.jsv.2013.09.043
29. Insperger T, Mann BP, Stépán G, Bayly PV (2003) Stability of up-milling and down-milling. Part 1: alternative analytical methods. Int J Mach Tools Manuf 43:25–34
30. Khasawneh FA, Mann B, Insperger T, Stépán G (2009) Increased stability of low-speed turning through a distributed force and continuous delay model. J Comput Nonlinear Dyn 4(4):041,003
31. Mann BP, Bayly PV, Davies MA, Halley JE (2004) Limit cycles, bifurcations, and accuracy of the milling process. J Sound Vib 277:31–48
32. Song Q, Ai X, Tang W (2011) Prediction of simultaneous dynamic stability limit of time-variable parameters system in thin-walled workpiece high-speed milling processes. Int J Adv Manuf Technol 55(9–12):883–889
33. Insperger T, Stépán G (2002) Semi-discretization method for delayed systems. Int J Numer Methods Eng 55:503–518
34. Insperger T, Stépán G (2004) Updated semi-discretization method for periodic delay-differential equations with discrete delay. Int J Numer Methods 61:117–141
35. Insperger T, Stepan G, Turi J (2008) On the higher-order semi-discretizations for periodic delayed systems. J Sound Vib 313:334–341
36. Eksioglu C, Kilic Z, Altintas Y (2012) Discrete-time prediction of chatter stability, cutting forces, and surface location errors in flexible milling systems. J Manuf Sci Eng 134(6):061,006
37. Khasawneh FA, Mann BP (2011) A spectral element approach for the stability of delay systems. Int J Numer Methods Eng 87(6):566–592. doi:10.1002/nme.3122
38. Yavari A, Sarkani S, Jr EM (2000) On applications of generalized functions to beam bending problems. Int J Solids Struct 37(40):5675–5705. doi:10.1016/S0020-7683(99)00271-1
39. Li H, Song G, Hou J, Li S, Wen B (2013) A stability analysis of turning process considering the workpiece as a timoshenko beam. J Vibroeng 15(4):1927–1939 Cited By (since 1996)0
40. Altintaş Y (2000) Manufacturing automation, 1st edn. Cambridge University Press, New York. doi:10.2277/0521659736
41. Otto A, Khasawneh F, Radons G (2015) Position-dependent stability analysis of turning with tool and workpiece compliance. Int J Adv Manuf Technol 79(9–12):1453–1463. doi:10.1007/s00170-015-6929-1
42. Otto A, Rauh S, Kolouch M, Radons G (2014) Extension of tlusty's law for the identification of chatter stability lobes in multi-dimensional cutting processes. Int J Mach Tools Manuf 82:50–58
43. Law M, Altintas Y, Phani AS (2013) Rapid evaluation and optimization of machine tools with position-dependent stability. Int J Mach Tools Manuf 68:81–90. doi:10.1016/j.ijmachtools.2013.02.003
44. Law,M, Phani AS, Altintas Y (2013) Position-dependent multibody dynamic modeling of machine tools based on improved reduced order models. J Manuf Sci Eng 135(2):021,008. doi:10.1115/1.4023453